Eur. Phys. J. Plus (2023) 138:603
https://doi.org/10.1140/epjp/s13360-023-04218-4

THE EUROPEAN PHYSICAL JOURNAL PLUS

Regular Article

Combined in situ XRF–LIBS analyses as a novel method to determine the provenance of central Mediterranean obsidians

Ilaria Costantini[1,a], **Marco Veneranda**[2], **Nagore Prieto-Taboada**[1], **Anna Maria De Francesco**[3], **Kepa Castro**[1], **Juan Manuel Madariaga**[1,4], **Gorka Arana**[1]

[1] Department of Analytical Chemistry, Faculty of Science and Technology, University of the Basque Country (UPV/EHU), 48080 Bilbao, Spain
[2] Department of Condensed Matter Physics, Crystallography and Mineralogy, University of Valladolid (UVa), Valladolid, Spain
[3] Department of Biology, Ecology and Earth Science, University of Calabria (UniCal), Cosenza, Italy
[4] Unesco Chair of Cultural Landscapes and Heritage, University of the Basque Country (UPV/EHU), Vitoria-Gasteiz, Spain

Received: 17 October 2022 / Accepted: 22 June 2023

Abstract This work presents a new calibration method for determining the provenance of obsidian artefacts based on the combined use of XRF and laser-induced breakdown spectroscopy (LIBS). At first, obsidian samples collected from the main Mediterranean sources were characterized using portable XRF and LIBS systems. After data treatment, elemental information was used to carry out principal component analysis (PCA) for each technique. Rb, Sr, Zr, Y and Fe elements, detected by using XRF, were found to be the key parameters enabling obsidians discrimination. Likewise, LIBS data helped differentiating the analysed patterns by the intensity of their main elemental components (Ca, Al, Mg and K). After selecting the key parameters detected by each technique, a new data matrix combining XRF and LIBS data was finally built. According to PCA results, the discrimination of Mediterranean sources based on combined XRF–LIBS data ensured a higher reliability over mono-analytical models, by increasing the Euclidean distance between sources projections over three-dimensional principal components plots. Knowing that the representativeness of elemental data could be compromised by the presence of superficial degradation products or deposition patinas, a shot-to-shot comparison of in-depth LIBS analyses is finally proposed as a method to disclose whether the spot under analysis was superficially contaminated or altered. Thus, the proposed strategy based on the combined use of portable XRF and LIBS spectrometers could be particularly useful for the in situ analysis of obsidian artefacts that underwent superficial alteration or could be covered by patina products.

1 Introduction

Since the Stone Age, obsidian represented an important resource to craft numerous kinds of weapons, tools and ornamental objects. Being a volcanic glass formed from rapidly cooled lava, the few major deposits known in ancient times represented an essential trading resource for nearby settlements [1, 2]. In the past few decades, the number of research works comparing the chemical–physical properties of archaeological artefacts with those of ancient obsidian sources outcrops significantly increased. As a result, analytical studies managed to reconstruct ancient trades routes and to extrapolate reliable information about the socio-economic contacts between cultures [1, 3]. For example, it has been analytically proved that obsidian artefacts were traded up to 900 km during the prehistoric period, thus revealing the occurrence of long-distance commercial contacts in the Mediterranean region [1].

Knowing that each obsidian outcrop presents a unique and very homogeneous chemical composition, comparative studies based on the characterization of major, minor and trace elements proved to be the ideal strategy to disclose the provenance of obsidian artefacts [4, 5]. Therefore, many obsidian provenance studies are nowadays based on the use of laser ablation inductively coupled plasma mass spectrometry (LA-ICP-MS) [6, 7]. This analytical technique allows to identify and quantify most elements, reaching detection limits in the order of parts per million (ppm) or billion (ppb). Source identification of obsidian objects from Italy [8], Japan [5], Syria [9], Yemen [10], Peru [11] and Argentina [12] (among others) amply demonstrates the effectiveness of this technique. However, being a benchtop instrument, LA-ICP-MS analyses can only be performed in the laboratory, which partially limits its applicability to the study of unmovable artefacts. Besides LA-ICP-MS, analytical protocols based on the interpretation of X-ray fluorescence (XRF) data have been successfully applied to obsidian sourcing for over two decades [3, 13, 14]. The main advantage of this analytical technique resides in the capability to qualify and semi-quantify the elemental composition of a target in a totally non-destructive way [15, 16]. As demonstrated by many publications on this topic, this analytical technique proved to effectively trace the origin of ancient obsidian artefacts found in the Mediterranean area [17–19] and further geographic regions [20–22]. More recently, laser-induced breakdown spectroscopy (LIBS) is also emerging as an useful analytical tool in the field of archaeological

[a] e-mail: ilaria.costantini@ehu.eus (corresponding author)

Published online: 10 July 2023

research [23, 24], although only one work focused on the provenance of obsidian so far [25]. Learning from other fields of research, the micrometric crater produced by the laser pulse makes that the LIBS technique can be used for depth-profiling analysis [26]. Indeed, by performing multiple laser shots on the same spot, the LIBS technique is able to remove the superficial layer of degradation and investigate the unaltered inner matrix. In the few cases in which obsidian artefacts undergo superficial alteration (e.g. hydration [27]) or could be covered by patina products (e.g. deposited during usage [28] or due to the exposure to the external environment [22]), the in-depth analysis of LIBS could represent a valuable analytical solution to overcome the issue of superficial alteration.

An additional advantage of XRF and LIBS techniques over other analytical provenance methods like LA-ICP-MS analysis resides in the availability of portable instruments [29–33] that can be used to carry out in situ analytical studies whenever obsidian artefacts cannot be either sampled or transferred to the laboratory. In the past decade, several studies confirmed the applicability of XRF portable instruments to the in situ study of obsidians provenance [17, 34, 35], while the only work so far based on the use of a portable LIBS system was published in 2019 [25].

As the combined use of LIBS and XRF has been successfully applied in other fields of research, the main objective of this work is to investigate the potential advantages provided by the combined use of these two complementary techniques in the field of obsidian provenance. Indeed, even though XRF spectrometers widely proved to effectively discriminate the source of obsidian artefacts, the LIBS technique could support XRF results by allowing depth-profiling analysis and providing a more efficient identification of light elements.

Being among the best studied and most well analysed in the world [14, 36, 37], central Mediterranean obsidian sources were selected as a representative case of study to test the combined use of portable XRF and LIBS spectrometers. In detail, the analytical work was organized as follows. First, portable XRF and LIBS systems were used to analyse obsidian samples from the main Mediterranean sources. Principal component analysis (PCA) [38] of spectroscopic results was then used to build mono-analytical discrimination models. After selecting the dominant key parameters detected by each spectroscopic system, XRF and LIBS results were combined to build a novel PCA-based discrimination model. The separation efficiency of the three proposed methods was then compared by measuring the Euclidean distances between averaged obsidian plot projections. A shot-to-shot comparison of in-depth LIBS analyses was finally evaluated as a method to verify the reliability of elemental results gathered from the study of altered obsidian artefacts.

2 Materials and methods

2.1 Obsidian samples

The Mediterranean area has several geological obsidian sources. Although mostly modest in size, the outcrops of obsidian are very numerous, but not all of them are glassy and of highly translucent quality. In Sardinia, the region of Monte Arci provides evidences of different Plio-Pleistocenic volcanic episodes which produced large amount of sub-alkaline rhyolites, during the first episode [39]. In the Monte Arci area, more sources and sub-sources have been recognized. As demonstrated on previous works, different methodologies were effectively employed to distinguish more than four geochemical groups in the obsidians of M. Arci (SA, SB1, SB2, SC1 and SC2) [19, 40–42]. Lipari is one of the seven Aeolian islands, all of volcanic origin, which had its cyclic volcanic activity from 270,000 years ago until 400 AD [43, 44]. On Lipari there are more obsidian outcrops of good quality, as Vallone Gabellotto and Canneto Dentro, but the only one that was exploited in the Neolithic period is that of the Vallone Gabellotto—Fiume Bianco, dated to a maximum of 11,400 and 8600 years BC by the fission track method [45, 46], which is visible as blocks in a thick deposit of pyroclasts. Palmarola is the westernmost of the Pontine Islands Archipelago, in the Gulf of Gaeta. It is formed by calc-alkaline volcanic rocks of Pliocene age. The formation of sodic rhyolitic domes occurred almost 1.7 Ma ago [47]. The Palmarola obsidian outcrops are along the southern slope of M. Tramontana [48] and next to Punta Vardella (as secondary deposits). The peralkaline character [49] of obsidian from Pantelleria, which is related to its genesis through fractioned crystallization by basaltic magma, allows to distinguish this source from all other Mediterranean obsidians (above all, by the content of Zr) [19].

Knowing that each obsidian source presents a very homogeneous chemical composition (data dispersion estimated in $\pm 1\%$ for most elements [50]), one representative sample was collected from each location and analyses were carried out in different spots.

2.2 Analytical instruments and data processing

For the spectroscopic characterization of obsidian patterns, portable instruments were used. On one side, X-ray fluorescence analyses were carried out by using a handheld XMET5100 spectrometer (Oxford Instruments, Oxford UK). The instrument is equipped with a rhodium anode X-ray tube and a silicon drift detector (energy resolution of 150 eV and spectral resolution of 20 eV), and the measurement spot has a diameter of 9 mm. For each sample, five spectra were acquired during 100 s (real time) to improve the limit of detection for the identification of trace elements.

On the other hand, LIBS analyses were performed using a portable EasyLIBS IVEA (model Easy 2C) system. This instrument employs a pulsed Nd:YAG laser, emitting at 1064 nm. The laser energy per pulse on the sample is 30 mJ with a repetition rate of 1 Hz and a duration of 5 ns. The beam is focused by a 15-cm focal length converging lens, which produces a spot of

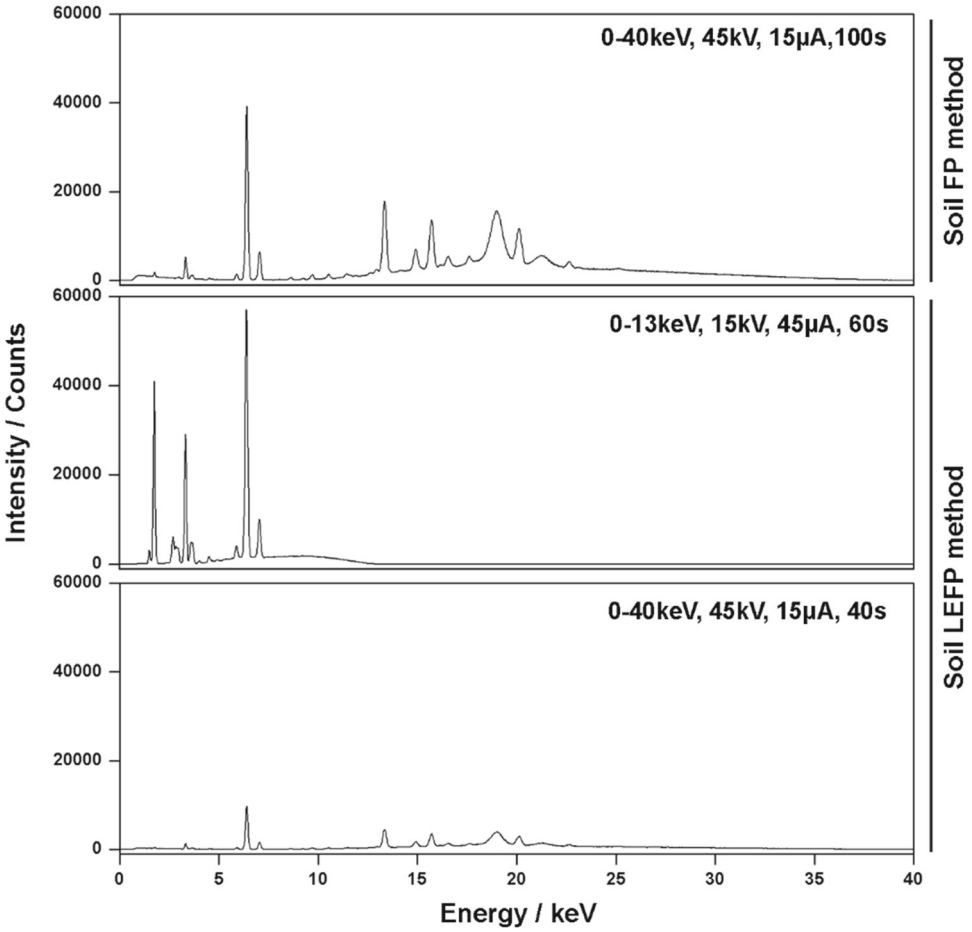

Fig. 1 Comparison between XRF spectra from Lipari's obsidian, gathered by setting SoilFP and SoilLEFP analytical modes. The three graphs have been represented using equal vertical scales (number of counts) to underline how spectral intensities varies according to the employed method

analysis of around 500 µm in diameter. The plasma signal is delivered by an optic probe to three spectrometers, covering the ultraviolet (UV, 196–419 nm), the visible (VIS, 420–579 nm) and the near-infrared (NIR, 580–1000 nm) spectral ranges, respectively (HR2000+/Ocean Optics, USA). In this work, measurements were performed with the double pulse mode by setting an optimized delay time of 50 µs to the laser pulse and a gate width of 5 ms. For each sample, five spectra (resolution of 0.2 nm) were collected by accumulating 30 laser shots from the same spot of analysis. The AnaLIBS 6.3 software was used for automatic spectra acquisition and visualization, while peaks identification was carried out using the NIST Atomic database [51].

After spectra acquisition, obsidian samples comparison was carried out taking into account the normalized intensity values of the main peak of each detected element. In the case of XRF spectra, the Kα line found at 1.74 (Si), 3.32 (K), 3.69 (Ca), 4.53 (Ti), 5.90 (Mn), 6.41 (Fe), 8.60 (Zn), 10.50 (As), 13.39 (Rb), 14.16 (Sr), 14.96 (Y), 15.8 (Zr) and 16.62 keV (Nb) was taken into consideration for the identification of Si, K, Ca, Ti, Mn, Fe, Zn, As, Rb, Sr, Y, Zr and Nb elements, respectively. Regarding LIBS spectra, the emission lines detected at 257.5 (Mn), 259.8 (Fe), 279.5 (Mg), 288.3 (Si), 334.8 (Ti), 393.2 (Ca), 396.0 (Al), 455.3 (Ba), 588.6 (Na), 766.0 (K) and 779.4 nm (Rb) were considered.

The IDAT/SpectPro software [52, 53] was used to treat and normalize all spectra, while the intensity value of elemental peaks was automatically calculated for each spectrum by using a dedicated MATLAB routine [54]. In this way, regardless of the analytical technique, each element will be represented by a numerical value comprised between 0 and 1. Normalized intensity values were finally analysed through the Unscrambler®7.6 software by using a multivariate method based on principal component analysis (PCA) [38].

The PCA converts the elemental values of the analysed data matrix into a new set of nonlinear variables called principal components (PC). Considering that PC1, PC2 and PC3 (which generally explain almost the totality of data variance) can be represented in a three-dimensional coordinate system, the separation among obsidian sources was evaluated by measuring their Euclidian distance in the Cartesian space. To do so, the following equation was used:

$$d(Oa, Ob) = \sqrt{(X_2 - X_1)^2 + (Y_2 - Y_1)^2 + (Z_2 - Z_1)^2} \quad (1)$$

where d is the distance between the two obsidians sources to be evaluated (Oa and Ob), while x, y and z are the numerical expression of the considered averaged obsidian projections over PC1, PC2 and PC3, respectively.

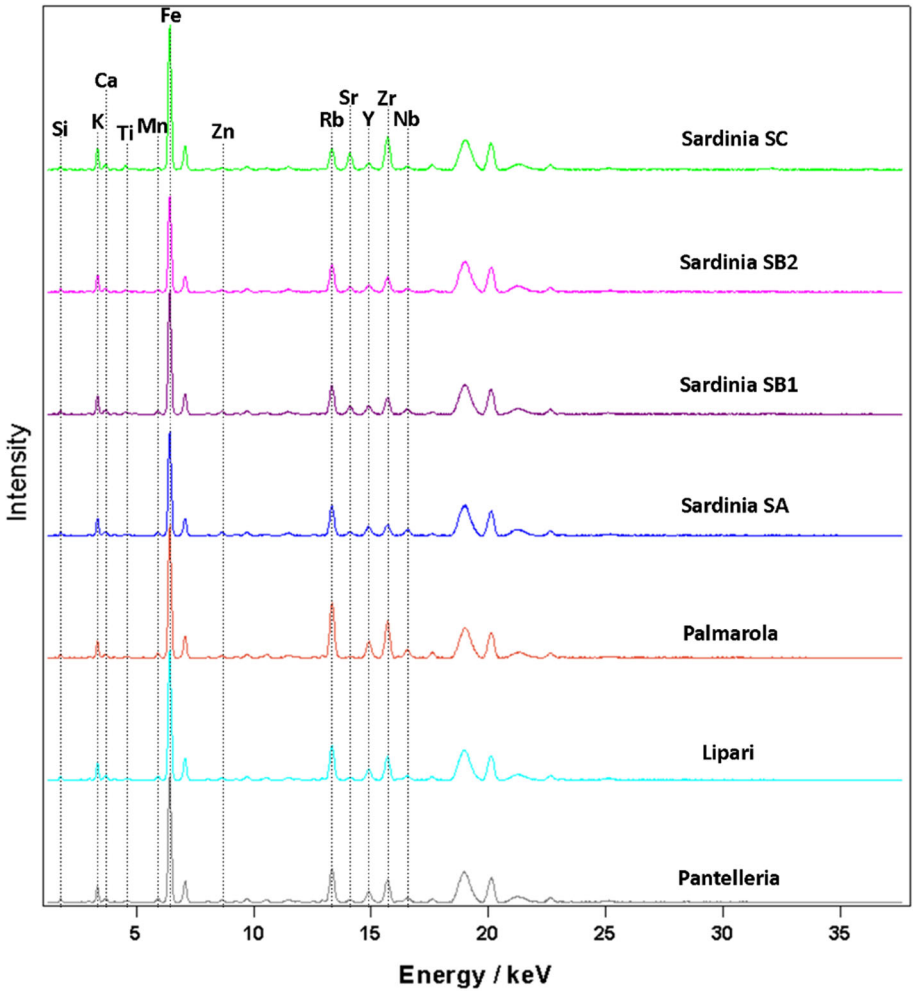

Fig. 2 Averaged XRF spectra collected from the study of obsidian patterns. Signals detected between 17 and 25 keV are attributed to the Compton and Rayleigh scattering lines [57]

3 Results

3.1 XRF discrimination model

The spectrometer used in this work is provided with different fundamental parameter (FP)-based methods to optimize the elemental identification and semi-quantification according to the target under analysis (soils, pure metals, alloys, etc.). For this reason, the first step of this work consisted in selecting the optimal method to characterize obsidian standards. Taking into account the experience gained in previous works [55], the spectra obtained using SoilFP and SoilLEFP methods were compared. On the one hand, acquisition parameters of SoilFP mode are optimized to maximize the detection of heavy elements ($Z > 18$). Thus, spectra are acquired over 100 s (spectral range between 0 and 40 keV) by setting a voltage of 45 kV and a current of 15 μA (see Fig. 1). On the other hand, by setting the SoilLEFP mode, the 100 s of acquisition is used to collect two different spectra. During the first 60 s, the spectrometer optimizes the detection of light elements (atomic number $Z < 18$) by emitting X-rays with a voltage of 15 kV and a current of 45 μA. The remaining 40 s are then used to capture a second spectrum by setting the same current and voltage conditions described for the SoilFP mode (see Fig. 1).

Knowing that obsidian sources can be mainly differentiated by their relative content of heavy elements as Rb, Sr, Y, Zr and Nb (Z between 36 and 41) [19, 56], SoilFP proved to be the optimal method to analyse the Mediterranean patterns.

After selecting the analytical method, five spectra per sample were collected. The comparison provided in Fig. 2 clearly highlights that, besides the $K\alpha$ peak of Fe (6.40 keV), the main differences among obsidian sources were found in the range between 13 and 17 keV, where the spectral features of Rb (13.40 keV), Sr (14.17 keV), Y (14.96 keV), Zr (15.78 keV) and Nb (16.62 keV) are present.

After observing clear spectral differences among obsidian patterns, all XRF spectra were normalized to the height of the Rh Lα Compton peak [58]. Afterwards, a MATLAB routine was used to extrapolate, from each spectrum, the intensity values of the main elemental peaks listed in Sect. 2.2. All values were then divided by the normalized intensity of the strongest peak (Ka line of Fe,

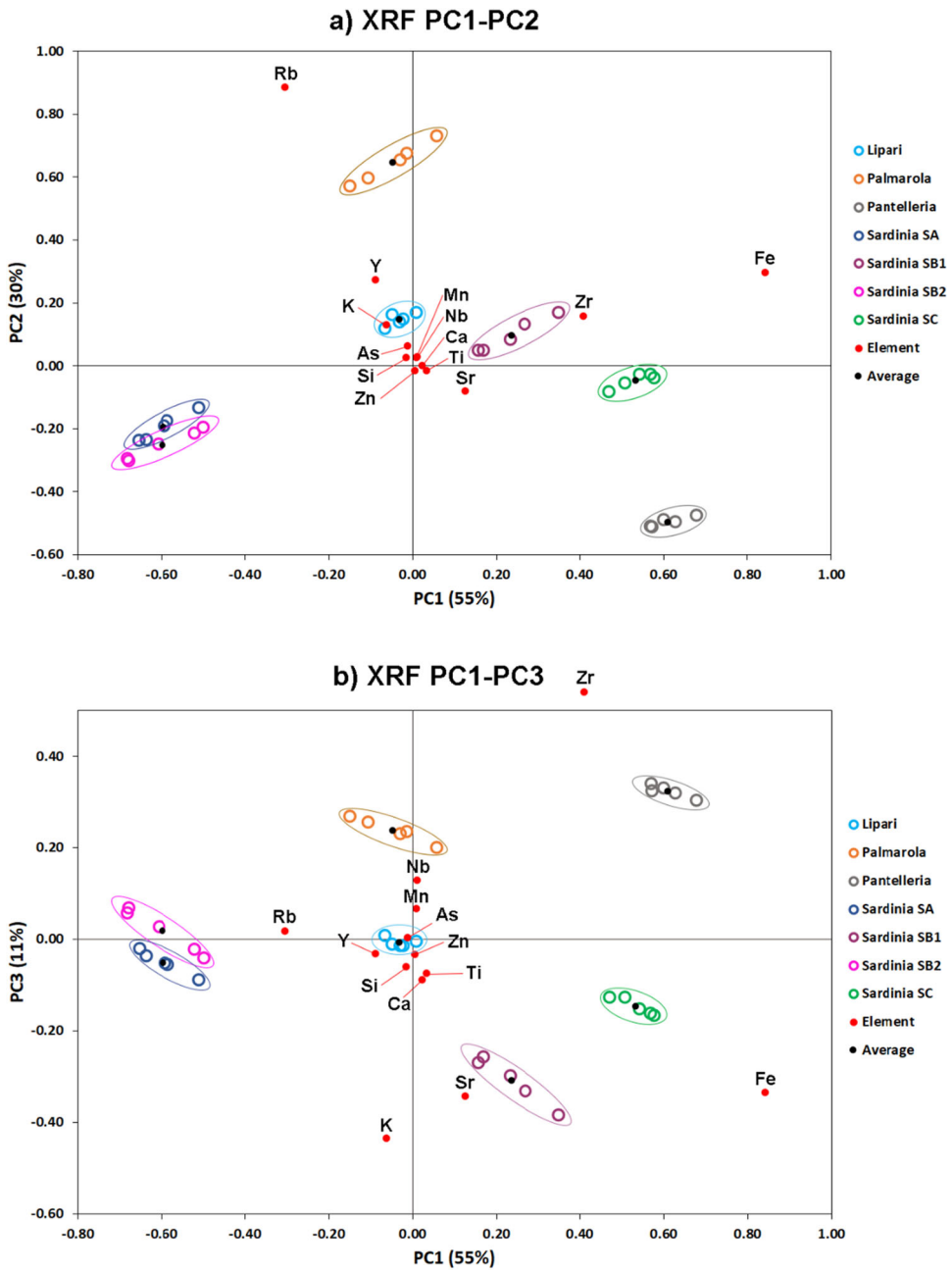

Fig. 3 Scores and loadings plots from the PCA of XRF data. a) PC1–PC2 and b) PC1–PC3 (Zr projection is out of scale: (+ 0.41; + 0.74). The variance explained by PC1 + PC2 + PC3 is 96%

from the fourth spectra of Sardinia SB1). In this way, a data matrix was created in which all elemental parameters are expressed by a value ranging between 0 and 1. The multivariate analysis of the data matrix was finally carried out using The Unscrambler 7.6 software.

As displayed by the score plots shown in Fig. 3, PCA results underlined a clear separation between most Mediterranean sources. In detail, the greatest variance in data projection lies on principal component 1 (PC1, 55%) and PC2 (30%). By associating scores position with loadings distribution (red dots), it was deduced that Rb, Fe, Y, Zr, Sr and K are the elemental variables that contribute the most to the separation of Mediterranean obsidians. Even though most sources were effectively discriminated, the proximity between SA (blue circles) and SB2 (magenta circles) projections over both PC1–PC2 and PC1–PC3 plots proved that XRF was not able to clearly separate the two clusters. Even though Sardinia SB1 (purple circles) and Lipari (light blue circles) clusters were found relatively close in the PC1–PC2 plots, their distance increases considerably by taking into consideration PC3. The PC values representing the five projections of each obsidian pattern were averaged and represented in the binary plots as black dots. As PC1, PC2 and PC3 (explaining 96% of data variance) can be represented as the axis of a *xyz* coordinate system, the separation among obsidian sources was measured by calculating their Euclidean distance in the three-dimensional space. As listed in Table 1, the calculated distance between Sardinia SA–Sardinia SB2 proved that the two obsidian varieties cannot be differentiated by the model.

Table 1 Three-dimensional Euclidean distances between averaged obsidian projections, calculated from the PCA of both mono-analytical and combined data matrixes

	Lipari	Palmarola	Pantelleria	Sardinia SA	Sardinia SB1	Sardinia SB2	Sardinia SC
XRF (96%)							
Lipari	0.00						
Palmarola	0.56	0.00					
Pantelleria	1.16	1.48	0.00				
Sardinia SA	0.87	1.18	1.77	0.00			
Sardinia SB1	*0.49*	0.87	1.02	1.24	0.00		
Sardinia SB2	0.89	1.21	1.75	*0.09*	1.27	0.00	
Sardinia SC	0.83	1.14	0.66	1.61	*0.47*	1.62	0.00
LIBS (96%)							
Lipari	0.00						
Palmarola	*0.22*	0.00					
Pantelleria	0.43	*0.23*	0.00				
Sardinia SA	*0.45*	*0.49*	0.58	0.00			
Sardinia SB1	0.64	0.70	0.84	*0.34*	0.00		
Sardinia SB2	*0.29*	*0.06*	*0.18*	0.52	0.74	0.00	
Sardinia SC	*0.38*	*0.18*	*0.25*	0.58	0.75	*0.14*	0.00
LIBS + XRF (89%)							
Lipari	0.00						
Palmarola	0.55	0.00					
Pantelleria	1.89	1.47	0.00				
Sardinia SA	1.72	2.11	2.62	0.00			
Sardinia SB1	2.24	2.62	3.23	1.52	0.00		
Sardinia SB2	0.98	0.80	1.25	1.86	2.80	0.00	
Sardinia SC	1.37	0.94	0.86	2.49	2.79	1.23	0.00

The percentages among parenthesis represent the cumulated data variance explained by PC1, PC2 and PC3. Lower values (below 0.5) are highlighted in italic

In addition to this, the Euclidian distances measured between Lipari–Sardinia SB1, and Sardinia SB1–Sardinia SC averaged values were also found to be particularly low (<0.5).

3.2 LIBS discrimination model

Complementarily to XRF data, additional LIBS analyses were performed. After selecting five spots of interest per sample, LIBS spectra were collected by accumulating the plasma generated by 30 consecutive laser pulses. The five spectra collected from each obsidian standard were then averaged using the IDAT/SpectPro software and represented in Fig. 4. Even though the three spectrometers cover a range between 190 and 1000 nm, Fig. 4 only displays the UV (between 230 and 480 nm) and IR (between 700 and 810 nm) sections, as the main emission lines of most elements are observed there. Similar to the XRF results, clear differences in the intensity of many emission lines were detected among the averaged LIBS spectra of Mediterranean obsidian standards.

After visual comparison, all LIBS spectra were normalized. Knowing that the silica content of Mediterranean standards is relatively constant (SiO between 73 and 75.5 wt% [19]) and that the Si emission lines were proved to be irrelevant parameters for LIBS-based provenance studies [25], all spectra were normalized to the height of the main emission line of Si (288.3 nm). All values were then divided by the normalized intensity of the strongest peak (Na line at 589.0 nm, from the second spectra of Sardinia SB1 standard). In this way, we obtained a data matrix in which all elemental parameters are expressed by values ranging between 0 and 1. As for the case of XRF, LIBS data matrix was finally analysed using a multivariate method based on PCA.

As displayed in Fig. 5, projected data are mainly resolved by Ca, Al, K and Mg elements, which are acknowledged for being the major components of obsidians' geochemistry [56]. This result underlines the complementarity between LIBS and XRF. Indeed, the high sensitivity of the LIBS technique towards the identification of alkaline and alkaline earth elements helped compensating the low sensitivity of XRF in the detection of light elements.

Binary plots provided in Fig. 5 proved that the degree of obsidians discrimination achieved by PCA of LIBS data was not as good as with XRF results. Indeed, as summarized in Table 1, the three-dimensional Euclidean distance between obsidian averaged projections was often low (below 0.5). In detail, Palmarola, Sardinia SB2 and SC samples cannot be differentiated by the plot of PC1 and PC2, which explain 82% of the total variance. Even though a better discrimination of Sardinia SC projections can be achieved by considering PC3 (11%), the measured Euclidian distances are still unsatisfactory.

However, it is important to underline that, unlike XRF, the PCA of LIBS data successfully differentiated Sardinia SA averaged projection from the Sardinia SB2 one (Euclidean distance = 0.52). Similarly, increased three-dimensional distances were measured between Lipari–Sardinia SB1 (0.64) and Sardinia SB1–Sardina SC (0.75). Therefore, this result highlights the complementary information provided by the two techniques when dealing to the discrimination of Mediterranean obsidians.

3.3 Combination of XRF and LIBS data

After confirming the complementarity between XRF and LIBS results, a new data matrix was built that combined the main discriminant variables detected by each technique. According to the PC plots displayed in Figs. 3 and 5, Rb, Sr, Zr, Y and Fe elements were considered as key parameters for XRF, while the intensity values of Al, K, Mg and Ca lines were considered for LIBS. Since both XRF and LIBS parameters were previously normalized to values ranging from 0 to 1, the values obtained for each technique were considered to have comparable statistical weight.

As displayed in Fig. 6, PCs gathered from the PCA of the combined XRF–LIBS data matrix ensured an improved separation of all obsidian clusters. Comparing the PCA of combined XRF–LIBS parameters with the results provided by the LIBS data matrix, the Euclidean distance measured between averaged obsidian projections increased in all the cases in a range that goes from + 148 to + 1160%.

Compared to XRF results, Euclidean distances improved in 71.5% of the cases (6 out of 21 combinations). As displayed in Table 1, the most evident improvements were obtained in the separation of obsidian clusters that, as explained in Sect. 3.1, were not well resolved by the PCA of the XRF data matrix. Thus, the Euclidean distance between averaged Sardinia SA and SB2 passed from 0.09 to 1.86 (+ 1982%), while the values between Lipari–Sardinia SB1 and Sardinia SB1–Sardinia SC passed from 0.49 to 2.24 (+ 360%) and from 0.47 to 2.70 (+ 590%), respectively.

The results described in this section proved again the advantages provided by the combination of XRF and LIBS data. Indeed, by selecting the key elemental parameters detected by each technique, it was possible to obtain a solid discrimination model that ensured an increased separation of obsidian's clusters over mono-analytical methods.

3.4 Shot-by-shot LIBS analysis

Besides the different sensitivity in elements detection, XRF and LIBS techniques also differ in the way they collect the spectral information from the target under analysis. Indeed, XRF performs non-destructive measurements by collecting elemental information from a bigger spot of analysis than LIBS systems (in our case, 9 mm vs. 0.5 mm diameter). This feature favours the use of XRF systems when it comes to the analysis of well-preserved obsidian artefacts, since the elemental information gathered from a larger area ensures a higher representativeness of the glass geochemistry. However, the bigger spot could be a disadvantage when superficial alterations

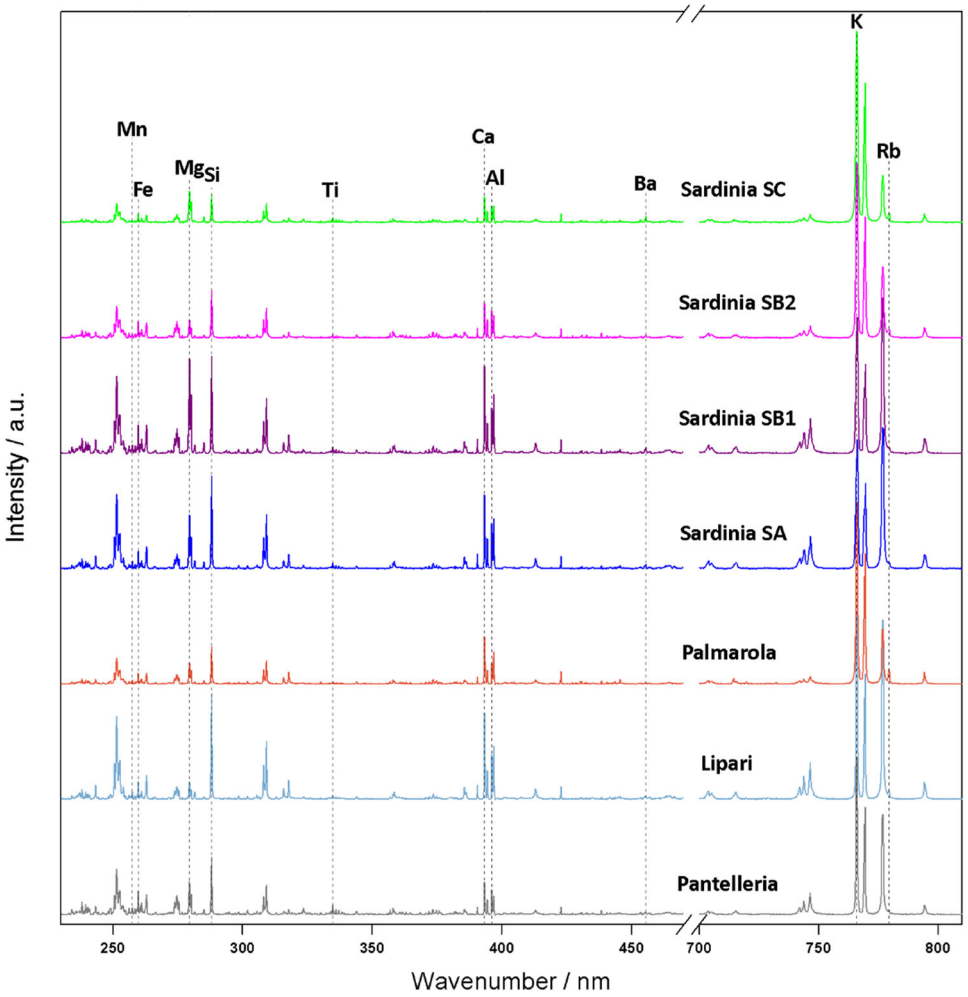

Fig. 4 Averaged LIBS spectra gathered from the study of obsidian standards

or deposition patinas are present. Indeed, it would increase the chances to intercept the detection of micrometric degradations, which would enrich the resulting spectra of specific elements, thus compromising the reliability of provenance studies. This is particularly problematic when the employed spectrometer is not coupled to a camera, since the operator cannot check the surface of the spot to be analysed. (This is the case of most commercial instruments, as the one used in this work.)

Compared to the non-destructive XRF, LIBS is a micro-invasive instrument that analyses the plasma generated by laser ablation. The higher the number of laser pulses accumulated from the same spot of interest, the deeper is the resulting crater (which is often not visible at the naked eye). Taking advantage of its micro-invasiveness, in-depth LIBS analyses can be used to discriminate the presence of superficial alteration products that cannot be discriminated by XRF measurements. Indeed, if the spot of interest presents superficial alterations or deposition patinas, the spectral comparison of LIBS shots accumulated from the same spot should reveal elemental fluctuations. Indeed, as consecutive laser shots would end penetrating the alteration layer, the peak intensity of the elements included in the degradation or deposition patina should decrease with increasing the depth of the analysed pulse. For the same reason, the intensity of Si lines should increase with depth, as it is the major component of obsidians.

To evaluate this hypothesis, shot-to-shot measurements in the same spot were performed and the spectra were compared to detect potential elemental fluctuations in obsidian standards when getting deeper shots. To do so, the intensity ratio of all detected elements was compared to the characteristic line of Si (288.3 nm).

Considering that each LIBS spectrum was obtained by accumulating 30 laser shots, elemental fluctuations were evaluated by averaging the intensity values of their characteristic lines every five consecutive shots. As shown in Fig. 7, the values obtained by averaging the most superficial shots (1–5) were in line with those measured at deeper pulses (26–30). The detection of constant intensity ratios proved the intensity of the detected elements was not affected by the presence of superficial alterations or deposition patinas. Averaged values and relative standard deviations are provided as supplementary material (Table SM1).

The negligible elemental fluctuations can be justified by the lack of alterations or deposition patinas on the surface of the analysed obsidian standard (from Lipari). However, when superficial products are present, elemental ratios should display decreasing intensities with depth. Knowing that key elemental parameters detected by LIBS (K, Mg, Ca and Al) are the ones most easily altered

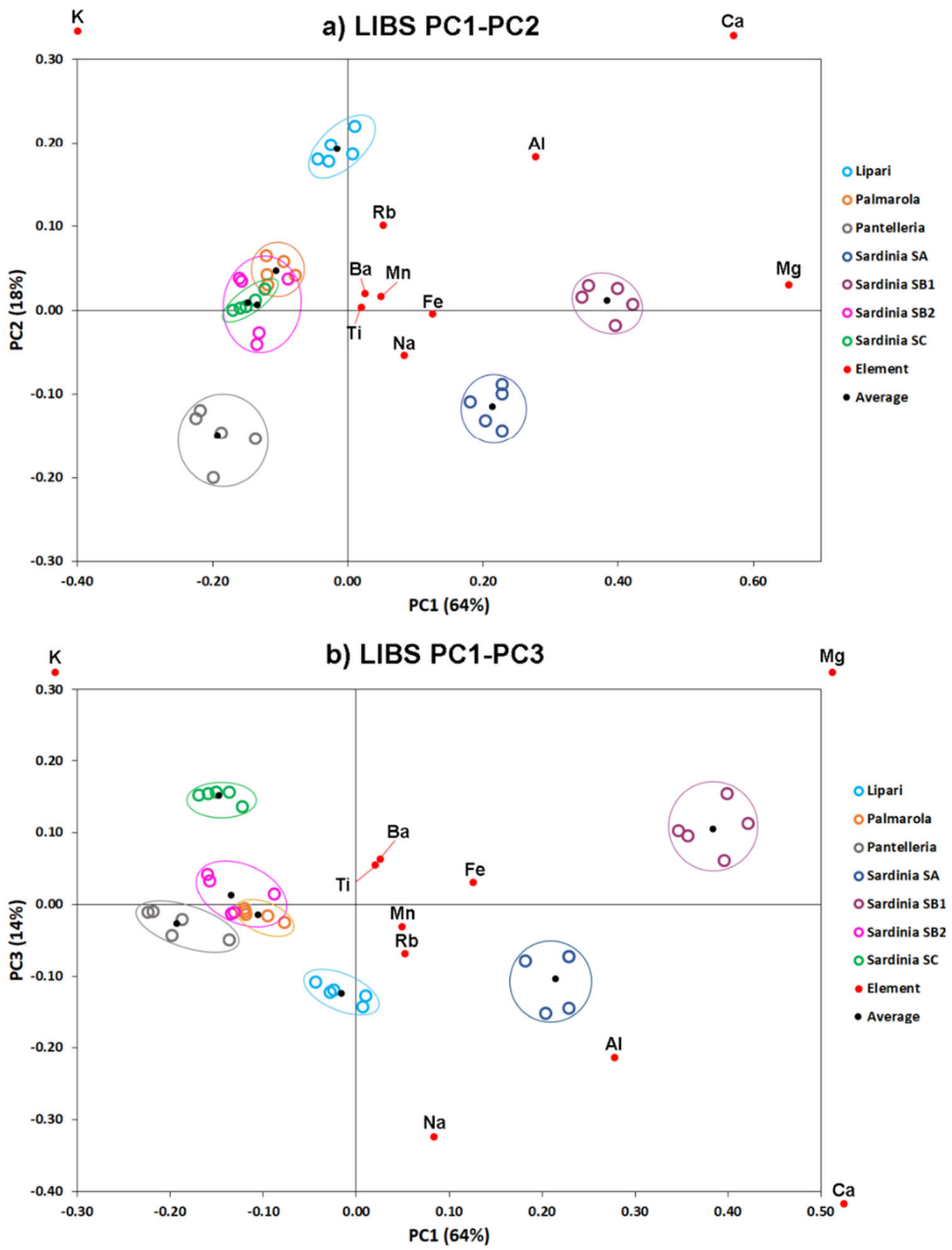

Fig. 5 LIBS score plot. K (−0.45; + 0.80), Ca (+ 0.52; + 0.55) and Mg (+ 0.65; − 0.03) variables have been represented outside the graph, as their projections were out of the scale of the PC1–PC2 plot. The same happened for K (−0.45; + 0.33), Mg (+ 0.65; + 0.72) and Ca (+ 0.52; −0.46) projections on the PC1-PC3 plot. The variance explained by PC1 + PC2 + PC3 is 96%

by the presence of alteration products (e.g., superficial salt deposits, as is the case of Pompeian mirrors [59]), this method could be used to rule out spurious spectra from the PCA analysis of the combined XRF–LIBS data matrix, thus further increasing the reliability of the discrimination method for provenance studies.

4 Conclusions

Obsidian fragments sampled from the central Mediterranean sources were analysed using two portable commercial instruments. After data collection, a MATLAB routine was used to extrapolate, from each spectrum, the normalized intensity values of the main characteristic peak of each detected element. Multivariate analyses of LIBS and XRF data matrixes were then carried out using the PCA method. The data plots provided in Fig. 3 show the portable XRF system was capable to correctly differentiate most obsidian sources, being Sardinia SA and SB2 the only varieties showing a reduced Euclidean distance. By associating scores position with loadings distribution (red dots), Rb, Fe, Y, Zr and Sr were found to be the main elemental variables contributing to the discrimination

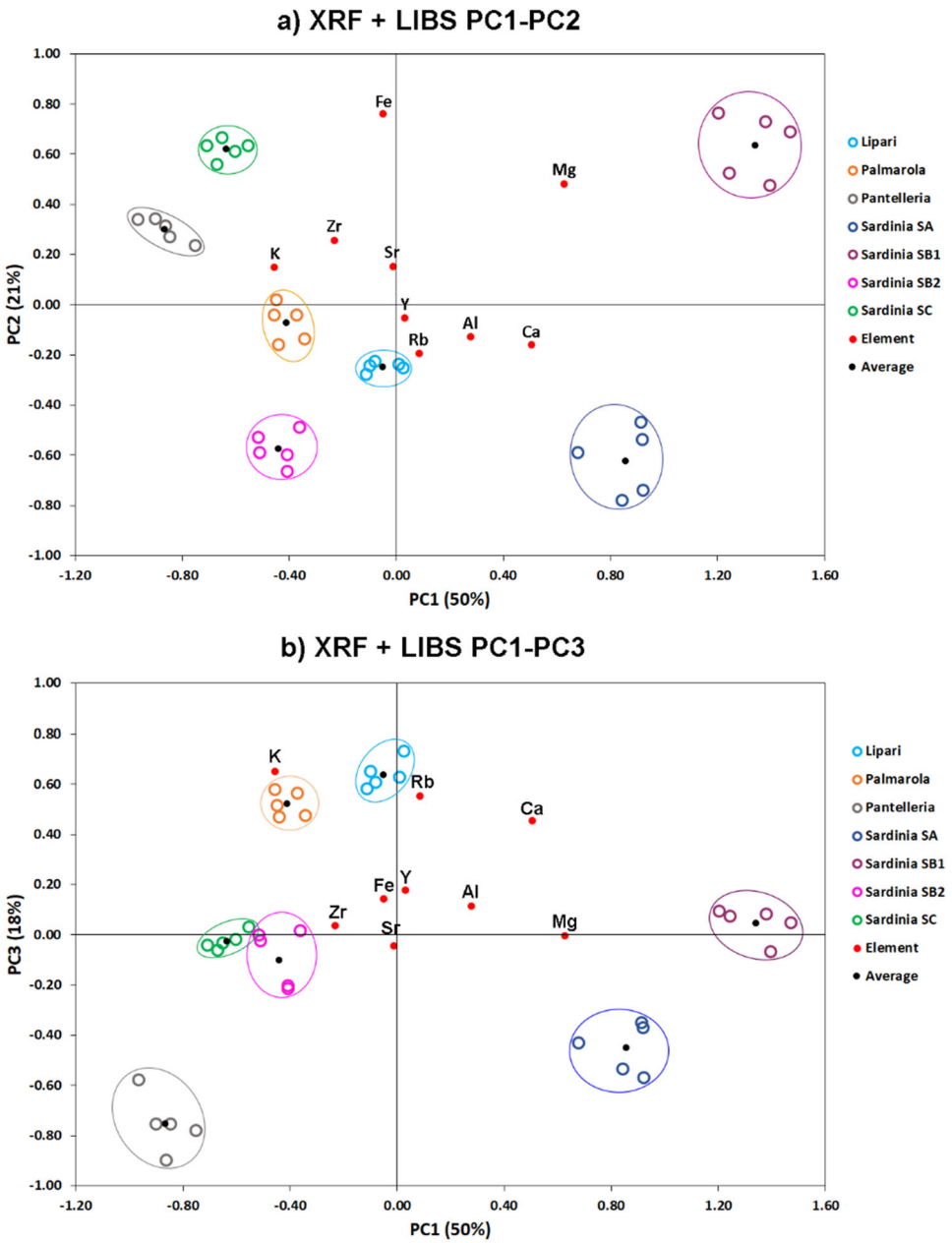

Fig. 6 Scores and loadings plots from the PCA of combined XRF–LIBS data. a) PC1–PC2 and b) PC1–PC3. The variance explained by PC1 + PC2 + PC3 is 89%

of Mediterranean sources. The reliability of XRF-based discrimination model can be attributed to the use of the SoilFP method, which adjusts the acquisition parameters to optimize the detection of heavy elements ($Z > 18$).

Unlike XRF, the use of portable LIBS instruments for obsidian provenance studies has been barely introduced. (The only paper focusing on this topic was published in 2019.) The results obtained in this work show this analytical technique could be of key importance for the in situ study of altered obsidian artefacts. Al, Mg, K and Ca were found to be the main LIBS parameters for the discrimination of obsidian standards, these being the main elements (besides Si) characterizing obsidians geochemistry. Although the calculated three-dimensional Euclidean distance between the analysed Mediterranean sources was often below XRF levels, the data plots provided in Fig. 5 show that LIBS data ensured a better discrimination of Sardinia SA and SB2 varieties over XRF results.

In order to increase the potential of the previous PCA models, a new data matrix that combines the key elemental parameters detected by XRF (Fe, Nb, Sr, Zr and Y) and LIBS (K, Mg, Al and Ca) was built. As proved by the PCA results provided in Fig. 7, combined XRF–LIBS data improved the discrimination of Mediterranean sources over mono-analytical models, ensuring a much higher Euclidean distances between obsidian clusters.

As well as providing elemental parameters that are complementary to XRF ones, the shot-to-shot analysis of LIBS depth profiling could be used to detect spectral contaminations caused by the presence of superficial degradation patinas. This makes the combined

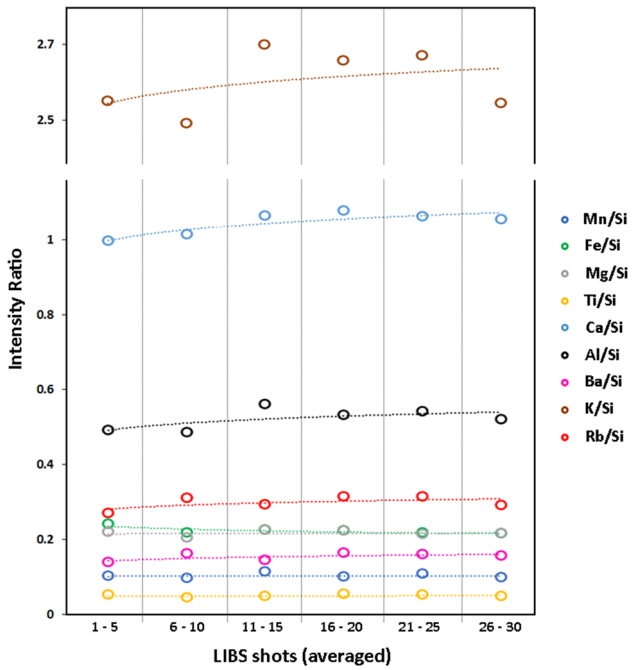

Fig. 7 Shot-to-shot evolution of elemental intensity ratios from the in-depth LIBS analysis of Lipari obsidian pattern

use of portable XRF and LIBS spectrometers a particularly useful strategy to apply for the in situ analysis of obsidian artefacts that underwent superficial alteration or could be covered by patina products.

Supplementary Information The online version contains supplementary material available at https://doi.org/10.1140/epjp/s13360-023-04218-4.

Acknowledgements This work has been financially supported by the DEMORA project (Grant No. PID2020-113391GB-I00), funded by the Spanish Agency for Research (through the Spanish Ministry of Science and Innovation (Grant No. BIA2017-870´63-P), MICINN, and the European Regional Development Fund (Grant No. BIA2017-870´63-P), FEDER). I. Costantini gratefully acknowledges to the UPV/EHU for her postdoctoral contract.

Funding Open Access funding provided thanks to the CRUE-CSIC agreement with Springer Nature.

Data Availability Statement All data generated or analysed during this study are included in this published article.

References

1. O. Williams-Thorpe, Archaeometry **37**, 217 (1995)
2. R.H. Tykot, J. Mediterr. Archaeol. **9**, 39 (1996)
3. R.H. Tykot, Acc. Chem. Res. **35**, 618 (2002)
4. L. Bellot-Gurlet, G. Poupeau, J. Salomon, T. Calligaro, B. Moignard, J.C. Dran, J.A. Barrat, L. Pichon, Nucl. Instrum. Methods Phys. Res. Sect. B Beam Interact. Mater. Atoms. **240**, 583 (2005)
5. S.C. Lynch, A.J. Locock, M.J.M. Duke, A.W. Weber, J. Radioanal. Nucl. Chem. **309**, 257 (2016)
6. B. Giussani, D. Monticelli, L. Rampazzi, Anal. Chim. Acta **635**, 6 (2009)
7. D. Barca, A.M. De Francesco, G.M. Crisci, J. Cult. Herit. **8**, 141 (2007)
8. F. Italiano, A. Correale, M. Di Bella, F.F. Martin, M.C. Martinelli, G. Sabatino, F. Spatafora, Mediterr. Archaeol. Archaeom. **18**, 151 (2018)
9. L. Khalidi, B. Gratuze, S. Boucetta, Archaeometry **51**, 879 (2009)
10. D. Barca, G. Lucarini, F.G. Fedele, Archaeometry **54**, 603 (2012)
11. L.C. Kellett, M. Golitko, B.S. Bauer, J. Archaeol. Sci. **40**, 1890 (2013)
12. C. Bellelli, F.X. Pereyra, M. Carballido, Geol. Soc. Spec. Publ. **257**, 241 (2006)
13. R.D. Giauque, F. Asaro, F.H. Stross, T.R. Hester, X-Ray Spectrom. **22**, 44 (1993)
14. R.H. Tykot, Appl. Sci. **11**, 7459 (2021)
15. A. De Francesco, M. Bocci, G.M. Crisci, in *X-Ray Fluorescence Spectrometry (XRF) in Geoarchaeology*. ed. by M.S. Shackley (Springer, New York, 2011), pp.81–107

16. Z. Kasztovszky, B. Maróti, I. Harsányi, D. Párkányi, V. Szilágyi, Quat. Int. **468**, 179 (2018)
17. E. Frahm, R. Doonan, V. Kilikoglou, Archaeometry **56**, 228 (2014)
18. M. Milić, J. Archaeol. Sci. **41**, 285 (2014)
19. A.M. De Francesco, G.M. Crisci, M. Bocci, Archaeometry **50**, 337 (2008)
20. F. Khademi Nadooshan, A. Abedi, M.D. Glascock, N. Eskandari, M. Khazaee, J. Archaeol. Sci. **40**, 1956 (2013)
21. D.D. Rindel, S.I. Perez, R. Barberena, B.L. MacDonald, M.D. Glascock, Archaeometry **62**, 1 (2020)
22. M. Giesso, H.G. Nami, J.J.Y. Capcha, M.D. Glascock, B.L. Macdonald, Archaeometry **62**, 215 (2020)
23. J.J. Remus, J.L. Gottfried, R.S. Harmon, A. Draucker, D. Baron, R. Yohe, Appl. Opt. **49**, 1990 (2010)
24. J.J. Remus, R.S. Harmon, R.R. Hark, G. Haverstock, D. Baron, I.K. Potter, S.K. Bristol, L.J. East, Appl. Opt. **51**, 65 (2012)
25. D. Syvilay, B. Bousquet, R. Chapoulie, M. Orange, F.X. Le Bourdonnec, J. Anal. At. Spectrom. **34**, 867 (2019)
26. D.M.D. Pace, N.A. Gabriele, M. Garcimuño, C.A. D'Angelo, G. Bertuccelli, D. Bertuccelli, Spectrosc. Lett. **44**, 399 (2011)
27. L.M. Anovitz, J. Archaeol. Sci. **26**, 735 (1999)
28. W.J. Stemp, A. Braswell, C.G.B. Helmke, J.J. Awe, J. Archaeol. Sci. Rep. **26**, 101859 (2019)
29. E. Frahm, R.C.P. Doonan, J. Archaeol. Sci. **40**, 1425 (2013)
30. A. Migliori, P. Bonanni, L. Carraresi, N. Grassi, P.A. Mandò, X-Ray Spectrom. **40**, 107 (2011)
31. S. Li, L. Liu, A. Yan, S. Huang, X. Huang, R. Chen, Y. Lu, K. Chen, Rev. Sci. Instrum. **88**, 023109 (2017)
32. G.S. Senesi, R.S. Harmon, R.R. Hark, in *Laser-Induced Breakdown Spectroscopy*, 2nd edn., ed. by J.P. Singh, S.N. Thakur (Elsevier, Amsterdam, 2020), pp.537–560
33. J. Rakovský, P. Čermák, O. Musset, P. Veis, Spectrochim. Acta Part B At. Spectrosc. **101**, 269 (2014)
34. I. Liritzis, N. Zacharias, in *Ray Fluorescence Spectrometry (XRF) in Geoarchaeology*. ed. by M.S. Shackley (Springer, New York, 2011), pp.109–142
35. R. Tykot, MRS Adv. **2**, 1769 (2017)
36. R.H. Tykot, Open Archaeol. **3**, 264 (2017)
37. R.H. Tykot, Open Archaeol. **5**, 83 (2019)
38. A. Tharwat, Int. J. Appl. Pattern Recognit. **3**, 197 (2016)
39. A. Montanini, M. Barbieri, F. Castorina, J. Volcanol. Geotherm. Res. **61**, 95 (1994)
40. R.H. Tykot, J. Archaeol. Sci. **24**, 467 (1997)
41. A.M. De Francesco, G.M. Crisci, in *Il primo popolamento Olocenico dell'area corsotoscana*, 1st edn., ed. by C. Tozzi, M.C. Weiss (ETS, Pisa, 1999), pp.253–258
42. A.M. De Francesco, M. Bocci, G.M. Crisci, in *Proceeding 2° Convegno Internazionale L'ossidiana Del Monte Arci Nel Mediterranean* (2004), pp. 303–309.
43. F. Forni, F. Lucchi, A. Peccerillo, C.A. Tranne, P.L. Rossi, M.L. Frezzotti, in *The Aeolian Islands Volcanoes*, 1st edn., ed. by F. Lucchi, A. Peccerillo, J. Keller, C.A. Tranne, P.L. Rossi (Geological Society of London, London, 2013), pp. 213–279
44. G. Bigazzi, F.P. Bonadonna, Nature **242**, 322 (1973)
45. A. Arias, G. Bigazzi, F.P. Bonadonna, M. Cipollini, J.C. Hadler, C.M.G. Lattes, G. Radi, in *Scientific Methodologies Applied to Works of Art*, 1st edn., ed. by P. Parrini (Montedison, Milan, 1986), pp.151–159
46. G. Bigazzi, M. Oddone, G. Radi, Archeometriai Muh. **1**, 1 (2005)
47. F. Barberi, S. Borsi, G. Ferrara, F. Innocenti, Mem. Della Soc. Geol. Ital. **17**, 581 (1967)
48. A. Cadoux, D.L. Pinti, C. Aznar, S. Chiesa, P.Y. Gillot, Lithos **81**, 121 (2005)
49. L. Civetta, Y. Cornette, G.M. Crisci, P.-Y. Gillot, G. Orsi, C.S. Requeios, Geol. Mag. **121**, 541 (1984)
50. R.G.V. Hancock, T. Carter, J. Archaeol. Sci. **37**, 243 (2010)
51. Y. Ralchenko, A. Kramida, Atoms **8**, 1 (2020)
52. G. Lopez-Reyes, J. Saiz, Á. Guzmán, A. Moral, C. Pérez, F. Rull, J.A. Manrique, J. Medina, in *European Planetary Science Congress 2018* (2018), pp. 1–2
53. M. Veneranda, J. Saiz, G. Lopez-reyes, J.A. Manrique, A. Sanz, C. Garcia-prieto, S.C. Werner, A. Moral, J.M. Madariaga, F. Rull, in *Europlanet Science Congress* (Virtual, 2020)
54. A.A.E. Fisher, J. Chem. Educ. **96**, 1502 (2019)
55. C. García-florentino, M. Maguregui, H. Morillas, I. Marcaida, J. Manuel, Microchem. J. **133**, 104 (2017)
56. M. Orange, F.X. Le Bourdonnec, A. Scheffers, R. Joannes-Boyau, Sci. Technol. Archaeol. Res. **2**, 192 (2016)
57. S. Pessanha, S. Silva, L. Martins, J.P. Santos, J.M. Silveira, J. Anal. At. Spectrom. **34**, 854 (2019)
58. V.D. Hodoroaba, V. Rackwitz, Anal. Chem. **86**, 6858 (2014)
59. M. Veneranda, S. Fdez-Ortiz de Vallejuelo, N. Prieto-Taboada, M. Maguregui, I. Marcaida, H. Morillas, A. Martellone, B. de Nigris, M. Osanna, K. Castro, J.M. Madariaga, Herit. Sci. **6**, 1 (2018)